

# A stabilization procedure for soil-water coupled problems using the element-free Galerkin method

T. Shibata<sup>a,\*</sup>, A. Murakami<sup>b</sup>

<sup>a</sup> Department of Civil and Environmental Engineering, Matsue College of Technology, 14-4 Nishi-ikuma, Matsue, Shimane 690-8518, Japan

<sup>b</sup> Graduate School of Agriculture, Kyoto University, Kitashirakawa Oiwake-cho, Sakyo-ku, Kyoto, Japan

## ARTICLE INFO

### Article history:

Received 23 February 2009

Received in revised form 12 January 2011

Accepted 25 February 2011

Available online 20 May 2011

### Keywords:

Stabilization procedure

Mesh-free method

Soil-water coupled problem

## ABSTRACT

The development of stability problems related to classical mixed methods has recently been observed. In this study, a soil-water coupled boundary-value problem, one type of stability problem, is presented using the element-free Galerkin method (EFG method). In this soil-water coupled problem, anomalous behavior appears in the pressure field unless a stabilization technique is used. The remedy to such numerical instability has generally been to adopt a higher interpolation order for the displacements than for the pore pressure. As an alternative, however, an added stabilization term is incorporated into the equilibrium equation. The advantages of this stabilization procedure are as follows: (1) The interpolation order for the pore pressure is the same as that for the displacements. Therefore, the interpolation functions in the pore pressure field do not reduce the accuracy of the numerical results. (2) The stabilization term consists of first derivatives. The first derivatives of the interpolation functions for the EFG Method are smooth, and therefore, the solutions for pore pressure are accurate. In order to validate the above stabilization technique, some numerical results are given. It can be seen from the results that a good convergence is obtained with this stabilization term.

© 2011 Elsevier Ltd. All rights reserved.

## 1. Introduction

In recent decades, the development of numerical computation technologies has enabled a variety of engineering problems to be solved and has brought about remarkable progress. Among the related findings, meshless and/or mesh-free methods in particular have been applied to some problems for which the usual finite element method is ineffective in dealing with significant mesh distortion brought about by large deformations, crack growth, and moving discontinuities.

Various meshless and/or mesh-free methods have been used for geotechnical problems, instead of the finite element method, to overcome the above-mentioned difficulties. Consolidation phenomena have been analyzed by means of element-free Galerkin method (EFG method) [1–4], the point/radial point interpolation method (PIM/RPIM) [5,6], the local RPIM [7], RKPM [8,9], and the natural neighbor method [10], the transient response of saturated soil has been dealt with under cyclic loading by means of EFG Method [11,12], wave-induced seabed response and instability have been examined by EFG Method [13] and RPIM [14,15], slip lines have been modeled by geological materials using EFG Method

[16], and a Bayesian inverse analysis has been carried out in conjunction with the meshless local Petrov-Galerkin method [17].

However, unless certain requirements are met in dealing with soil-water coupled problems for the finite element computation, based on the coupled formulation becoming ill-conditioned, numerical instabilities will occur [18]. The cause of this phenomenon is the over-constrained system of the equation. A widely used technique to overcome the instabilities consists in the coupled formulation. However, it is well known that not all the approximations lead to fully convergent solutions like soil-water coupled problems. In order to overcome these weaknesses, several strategies have been proposed [19,20]. For example, as a necessary condition for stability, the interpolation degree of the displacement field must be higher than that of the pore pressure field. In an equilibrium equation, displacement has derivatives that are one order higher than pore water pressure. For the displacement-pore water pressure mixed mode, equal-order interpolation is not consistent because it validates the Babuska-Brezzi condition or the much simpler path test proposed by Zienkiewicz and Taylor. An alternative means of stabilization was also proposed based on the Simo-Rifai enhanced strain method which even allows an equal order of interpolation degree for both variables.

However, these strategies are not directly applicable to meshless/mesh-free methods, because all the nodal points simultaneously have the same degree of freedom for both the

\* Corresponding author. Tel.: +81 852 36 5260; fax: +81 852 36 5218.

E-mail address: [shibata@matsue-ct.jp](mailto:shibata@matsue-ct.jp) (T. Shibata).

displacement field and the pore pressure field, and no information between the element and the nodes can be utilized.

Only a few attempts have been made, e.g., the backward Euler scheme for RPIM could be used to avoid spurious oscillation [21], and an unequal-order RPIM was introduced to alleviate numerical oscillation and improve accuracy for solution. In the latest literature, a three-point approximation technique with a variable time step has been proposed to avoid spurious ripple effects [22], and the stable EFG procedures considering Lagrange multipliers have also been presented [23]. The question of how a stabilization scheme should be developed with meshless methods is still an open topic.

The purpose of this paper is to present a stabilization methodology for the mesh-free analysis of soil-water coupled problems by incorporating the stabilizing term into the weak form. The advantage of this procedure is that the interpolation functions in the pore pressure field do not reduce the accuracy of the numerical results. Moreover, the methodology is similarly applicable to other coupled problems using EFG.

The following sections deal with descriptions of the formulation, an analysis of the bench mark test, and a foundation subjected to continuous loading within the framework of finite strain. Section 2 presents the formulation, including the stabilization term. In Section 3, two applications of the strategy to soil-water coupled problems are analyzed, one being the saturated soil column test appearing in Mira et al. [20], to demonstrate the effectiveness of the strategy, and the other being the foundation behavior under a displacement-controlled condition, for which the feasibility of the analysis will be thoroughly discussed. The conclusion follows in Section 4.

## 2. Formulation

The governing equations for soil-water coupled problems with boundary conditions and initial conditions are given as follows:

### 2.1. Governing equations

#### (a) Continuous equilibrium equation

$$\int_V \text{div} \dot{\mathbf{S}}_t dV + \rho_w (\int_V \text{tr} \mathbf{D} dV) \mathbf{b} = 0, \quad \dot{\mathbf{S}}_t = \dot{\mathbf{T}} + (\text{tr} \mathbf{D}) \mathbf{T} - \mathbf{T} \mathbf{L}^T \tag{1}$$

where  $\dot{\mathbf{S}}_t$  is the nominal stress rate,  $\rho_w$  is the density of water,  $\mathbf{b}$  is the body force per unit mass,  $\mathbf{T}$  is the total Cauchy stress,  $\dot{\mathbf{T}}$  is the Cauchy stress rate,  $\mathbf{L}$  is the velocity gradient,  $\mathbf{D}$  is the stretching, and  $V$  is the domain.

#### (b) Effective stress concept

$$\mathbf{T} = \mathbf{T}' - p_w \mathbf{I} \tag{2}$$

where  $\mathbf{T}'$  is the effective stress,  $p_w$  is the pore water pressure, and  $\mathbf{I}$  is the unit tensor.

#### (c) Constitutive equation

$$\dot{\mathbf{T}}' = L[\mathbf{D}] \tag{3}$$

where  $\dot{\mathbf{T}}'$  is the Jaumann rate of the effective stress.

#### (d) Continuity condition of soil-water coupled problems

$$\text{tr} \mathbf{D} + \text{div} \mathbf{v}_w = 0 \tag{4}$$

where  $\mathbf{v}_w$  is the average velocity of the pore water and the above equation is derived under the assumption that the skeleton grains and the pore fluid are incompressible.

#### (e) Darcy's law

$$\mathbf{v}_w = -k \mathbf{I} \text{grad} h_w \tag{5}$$

where  $k$  is the permeability and  $h_w$  is the total head.

#### (f) Boundary conditions

$$\begin{aligned} \dot{\mathbf{S}}_t \mathbf{n} &= \bar{\mathbf{s}}_t \text{ on } \Gamma_t \\ \mathbf{v} &= \bar{\mathbf{v}} \text{ on } \Gamma_v \\ \bar{q} &= \bar{\mathbf{v}}_w \cdot \mathbf{n} \text{ on } \Gamma_q \\ h_w &= \bar{h}_w \text{ on } \Gamma_h \end{aligned} \tag{6}$$

where  $\mathbf{n}$  is the unit normal vector at the boundary,  $\bar{\mathbf{s}}_t$  is the boundary value of the traction,  $\mathbf{v}$  is the velocity,  $\bar{\mathbf{v}}$  is the boundary value of the velocity,  $\bar{q}$  is the discharge per unit area with units of length per time,  $\bar{h}_w$  is the boundary head,  $\bar{\mathbf{v}}_w$  is the boundary velocity of the pore water,  $\Gamma_t$  is the stress boundary,  $\Gamma_v$  is the velocity boundary,  $\Gamma_q$  is the discharge boundary, and  $\Gamma_h$  is the hydraulic boundary.

#### (g) Initial conditions

$$\begin{aligned} \mathbf{T}' &= \mathbf{T}'|_{t=0} \text{ in } V \\ h_w &= h_w|_{t=0} \text{ in } V \end{aligned} \tag{7}$$

### 2.2. Constitutive equation

Herein, we briefly describe the Cam-clay model for finite strain according to Asaoka et al. [24]. It is firstly assumed that stretching tensor  $\mathbf{D}$  is divided into elastic and plastic components.

$$\mathbf{D} = \mathbf{D}^e + \mathbf{D}^p \tag{8}$$

The total volume change of the soil skeleton is expressed with the above two terms:

$$\int_0^t \text{tr} \mathbf{D} d\tau = \int_0^t \text{tr} \mathbf{D}^e d\tau + \int_0^t \text{tr} \mathbf{D}^p d\tau \tag{9}$$

where  $J = \det \mathbf{F} = \frac{1+e}{1+e_0}$ ,  $\mathbf{F}$  is the deformation gradient tensor, and  $1+e$  and  $1+e_0$  are the specific volumes at current time  $t$  and reference time  $t=0$ , respectively. The first term in the above equation is written in the following form:

$$\int_0^t \text{tr} \mathbf{D}^e d\tau = -\frac{\tilde{\kappa}}{1+e_0} \ln \frac{p'}{p'_0} \tag{10}$$

where  $p'$  and  $p'_0$  are the mean effective stresses at the current and the reference states, respectively, and  $\tilde{\kappa}$  is the swelling index.

The total volume change of a soil skeleton should be independent of the stress path according to Henkel [25], and it is a function of only the initial and the current effective stresses. This is expressed as the sum of the isotropic compression term and the one due to dilatancy, as seen in Ohta [26]:

$$\int_0^t \text{tr} \mathbf{D} d\tau = -\frac{\tilde{\lambda}}{1+e_0} \ln \frac{p'}{p'_0} - D \frac{q}{p'} = -\frac{\tilde{\lambda}}{1+e_0} \ln \frac{p'}{p'_0} - \frac{\tilde{\lambda} - \tilde{\kappa}}{M(1+e_0)} \frac{q}{p'} \tag{11}$$

where  $\tilde{\lambda}$  is the compression index,  $q$  is the second invariant of deviatoric stress,  $D$  is the dilatancy parameter,  $D = \frac{\tilde{\lambda} - \tilde{\kappa}}{M(1+e_0)}$ , and  $M$  is the critical state parameter.

By subtracting Eq. (10) from Eq. (11), we have the following well-known Cam-clay yield function:

$$f(p', q) = MD \ln \frac{p'}{p'_0} + D \frac{q}{p'} + \int_0^t \text{tr} \mathbf{D}^p d\tau = 0 \tag{12}$$

The rate type of constitutive equation for the Cam-clay model can be written as

$$\dot{\mathbf{T}}' = \left( \tilde{K} - \frac{2}{3} \tilde{G} \right) (\text{tr} \mathbf{D}) \mathbf{I} + 2\tilde{G} \mathbf{D} - \frac{\left( \frac{\tilde{G}}{\tilde{\kappa}} S - \tilde{K} \tilde{\beta} \mathbf{I} \right) \left( \frac{\tilde{G}}{\tilde{\kappa}} S \cdot \mathbf{D} - \tilde{K} \tilde{\beta} (\text{tr} \mathbf{D}) \right)}{\tilde{G} + \tilde{K} \tilde{\beta}^2 + h} \tag{13}$$

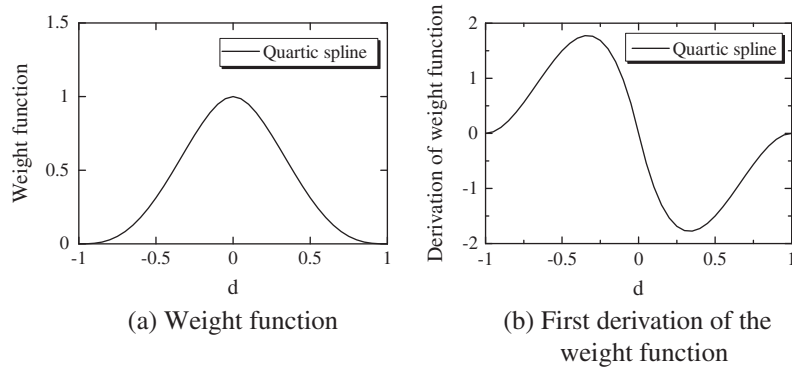


Fig. 1. Shape of the weight function.

Table 1  
Order of the interpolation function in FEM.

Number		0–1	1–1	1–2	2–2
Order	Pressure	0	1	1	2
	Displacement	1	1	2	2
■: Pressure ○: Displacement					

where

$$\tilde{K} = \frac{1+e}{\tilde{k}} p', \quad \tilde{G} = \frac{3(1-2\nu)}{2(1+\nu)} \tilde{K}, \quad \tilde{\beta} = \frac{1}{\sqrt{3}} \left( M - \frac{q}{p'} \right),$$

$$\tilde{\tau} = \frac{q}{\sqrt{3}}, \quad h = \frac{J p' \tilde{\beta}}{\sqrt{3} D}$$

2.3. Moving least squares approximant

In this study, the element-free Galerkin method (EFG method) is adopted. In the EFG Method, the interpolation functions are derived by the moving least squares approximant. In the moving least squares technique, approximation  $u^h(\mathbf{x})$  is expressed as

$$u^h(\mathbf{x}) = \mathbf{p}^T(\mathbf{x}) \mathbf{a}(\mathbf{x}) \tag{14}$$

where  $\mathbf{p}(\mathbf{x})$  is a complete polynomial basis of the arbitrary order and  $\mathbf{a}(\mathbf{x})$  are coefficients which are functions of space coordinates  $\mathbf{x}^T = [\mathbf{x}, \mathbf{y}]$ . A linear polynomial basis is adopted for all the calculations, namely,

$$\mathbf{p}^T(\mathbf{x}) [1, \mathbf{x}, \mathbf{y}] \tag{15}$$

Moving least squares interpolant  $u^h(\mathbf{x})$  is defined in the circle of the domain influence, referred to as the support. In order to determine the form for  $\mathbf{a}(\mathbf{x})$ , weighted discrete error norm  $J(\mathbf{x})$  is constructed and minimized.

$$J(\mathbf{x}) = \sum_{I=1}^n w_I(\mathbf{x}) [\mathbf{p}^T(x_I) \mathbf{a}(\mathbf{x}) - u_I]^2 \tag{16}$$

where  $w_I(\mathbf{x}) = w(\mathbf{x} - \mathbf{x}_I)$  is a weight function,  $n$  is the number of nodes within the circle, and  $u_I$  is the nodal value of  $u$  at  $\mathbf{x} = \mathbf{x}_I$ . The minimization condition requires

$$\frac{\partial J}{\partial \mathbf{a}} = 0 \tag{17}$$

which results in the following linear equation system:

$$\mathbf{A}(\mathbf{x}) \mathbf{a}(\mathbf{x}) = \mathbf{B}(\mathbf{x}) \mathbf{u}^T \tag{18}$$

where

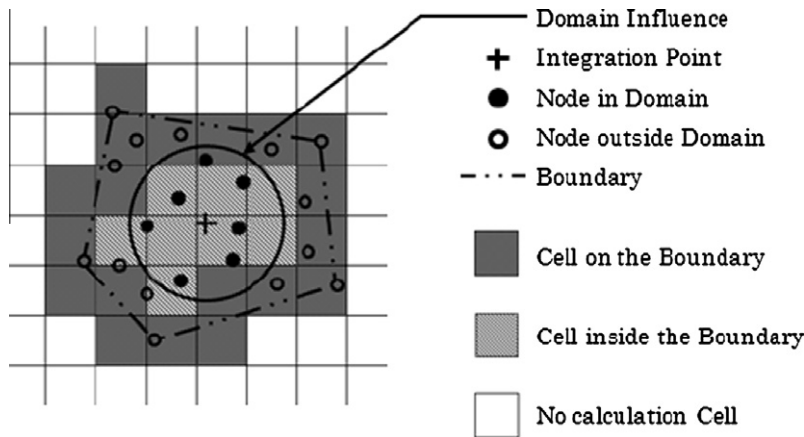


Fig. 2. Background cell and radius of the support.

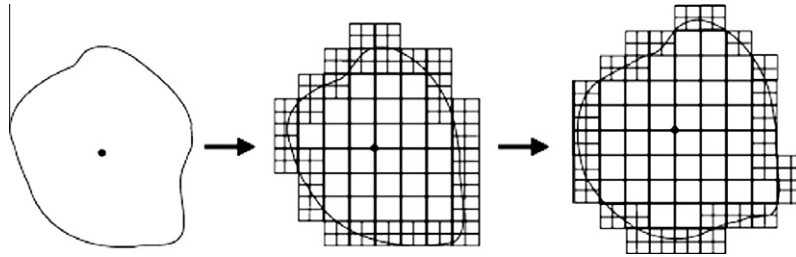


Fig. 3. Rearrangement and allocation of background cells to cover the changing domain.

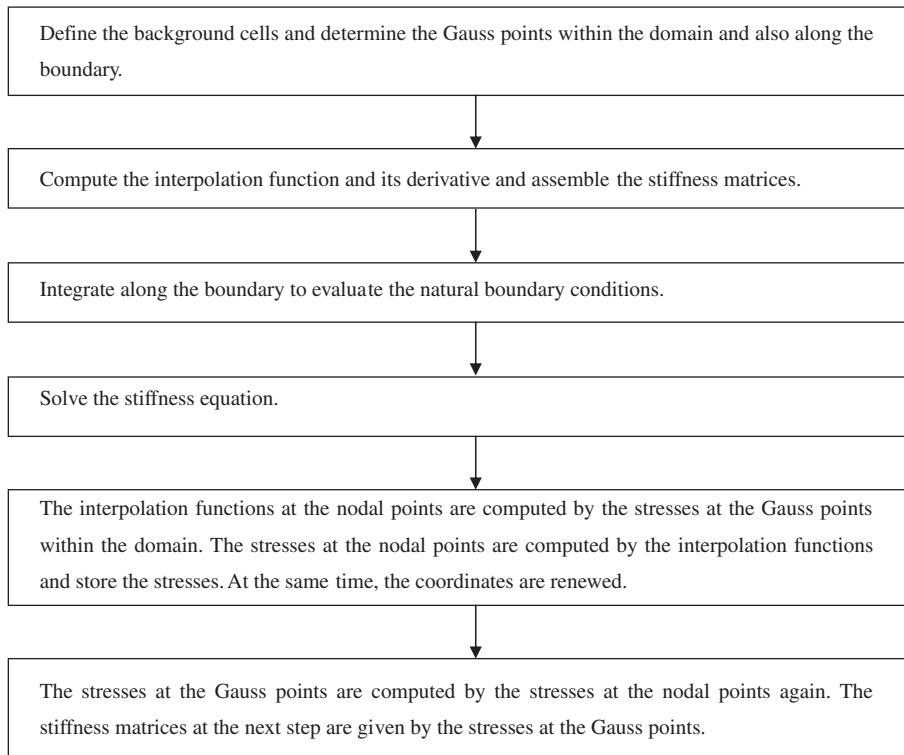


Fig. 4. Numerical implementation of the stresses.

$$\mathbf{A}(\mathbf{x}) = \sum_{I=1}^n w_I(\mathbf{x}) \mathbf{p}(\mathbf{x}_I) \mathbf{p}^T(\mathbf{x}_I),$$

$$\mathbf{B}(\mathbf{x}) = [w_1(\mathbf{x})\mathbf{p}(\mathbf{x}_1), w_2(\mathbf{x})\mathbf{p}(\mathbf{x}_2), \dots, w_n(\mathbf{x})\mathbf{p}(\mathbf{x}_n)],$$

$$\mathbf{u}^T = [u_1, u_2, \dots, u_n].$$

Solving the above equation for  $\mathbf{a}(\mathbf{x})$ , we obtain

$$\mathbf{a}(\mathbf{x}) = \mathbf{A}^{-1}(\mathbf{x}) \mathbf{B}(\mathbf{x}) \mathbf{u}^T \tag{19}$$

Substituting the above equation back into Eq. (14) leads to

$$u^h(\mathbf{x}) = \mathbf{p}^T(\mathbf{x}) \mathbf{A}^{-1}(\mathbf{x}) \mathbf{B}(\mathbf{x}) \mathbf{u}^T \equiv \mathbf{N}(\mathbf{x}) \mathbf{u}^T \tag{20}$$

where  $\mathbf{N}(\mathbf{x})$  is the interpolation function. The weight function used in this study is the quartic spline presented in Fig. 1. It strictly shows the functions of  $d = |\mathbf{x} - \mathbf{x}_I|$  in multiple dimensions as follows:

Quartic spline weight function

$$w(d) = 1 - 6\left(\frac{d}{d_m}\right)^2 + 8\left(\frac{d}{d_m}\right)^3 - 3\left(\frac{d}{d_m}\right)^4, \quad 0 \leq d \leq d_m$$

$$w(d) = 0, \quad d > d_m \tag{21}$$

where  $d_m$  is the radius of the support of  $w(d)$ . Note that the weight function and the first derivatives of its function are continuous at every point, as shown in Fig. 1.

#### 2.4. Setup of the stiffness equation

A set of the weak forms of the previous governing equations is discretized within the framework of EFG Method using the MLS approximated interpolation functions under the Cam-clay model. The principle of virtual work, through consideration of the boundary conditions, is given as

$$\int_V \text{div} \dot{\mathbf{S}}_t \cdot \delta \mathbf{v} \, dV + \int_{\Gamma_u} \rho(\mathbf{v} - \bar{\mathbf{v}}) \cdot \delta \mathbf{v} \, dS = 0 \tag{22}$$

$$- \int_V (\text{tr} \mathbf{D}) \delta h_w \, dV + \int_V v_w \cdot \text{grad} \delta h_w \, dV - \int_{\Gamma_q} \bar{q} \delta h_w \, dS - \int_{\Gamma_h} \beta(p_w - \bar{p}_w) \delta h_w \, dS = 0 \tag{23}$$

where  $\rho$  and  $\beta$  are Lagrange multipliers and  $\delta$  is the variational operator. Eqs. (22) and (23) express the equilibrium and the continuity of the pore water, respectively. The second term on the left side of Eq. (22) and the fourth term on the left side of Eq. (23) are the boundary conditions.

Here, the displacement rate and the head of the pore water are expressed as follows using the interpolation function of EFG:

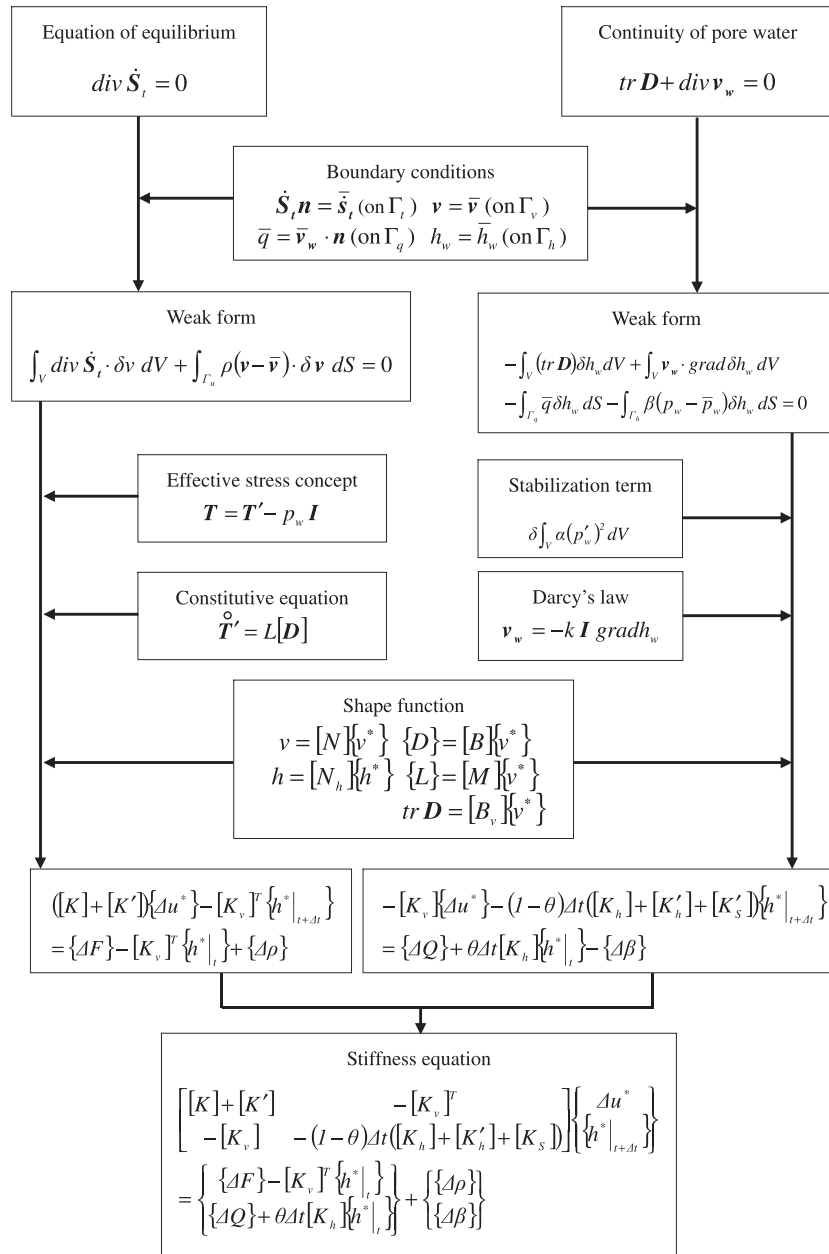


Fig. 5. Summary of the formulation.

$$v = \begin{bmatrix} N^1 & 0 & \dots & N^\alpha & 0 \\ 0 & N^1 & \dots & 0 & N^\alpha \end{bmatrix} \begin{Bmatrix} v_x^{*1} \\ v_y^{*1} \\ \vdots \\ v_x^{*\alpha} \\ v_y^{*\alpha} \end{Bmatrix} = [N] \{v^*\} \quad (24)$$

$$h_w = \frac{p_w}{\gamma_w} + \Omega = [N_h^1 \dots N_h^\beta] \begin{Bmatrix} h^{*1} \\ \vdots \\ h^{*\beta} \end{Bmatrix} = [N_h] \{h^*\} \quad (25)$$

where  $[N]$  and  $[N_h]$  are called the shape matrices,  $\Omega$  is the potential head,  $\gamma_w$  is the unit weight,  $\{v^*\}$  is the velocity and  $\{h^*\}$  is the total head at the nodal point.

Next, the following form is obtained as the stiffness equation:

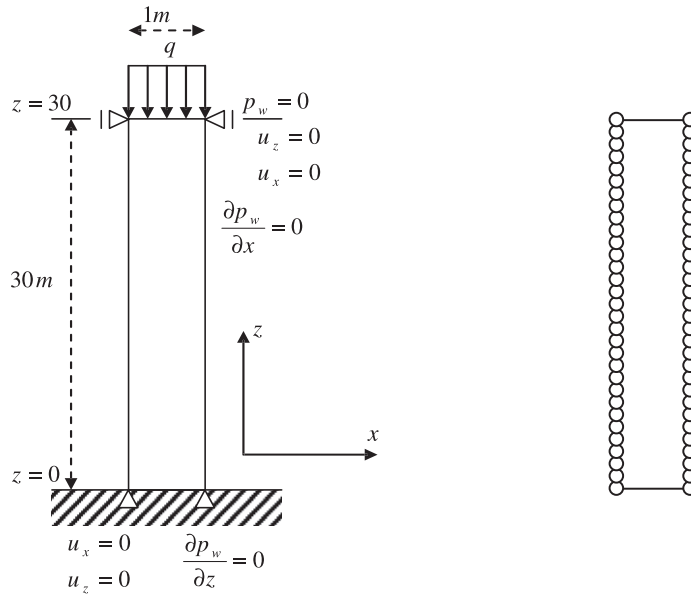
$$([K] + [K']) \{\Delta u^*\} - [K_v]^T \{h^*\}_{t+\Delta t} = \{\Delta F\} - [K_v]^T \{h^*\}_t + \{\Delta \rho\} \quad (26)$$

where

$$[K] = \int_V ([B]^T [C] [B] + [B]^T \{T'\} [B_v] - 2[B]^T [T^{***}] [B] + [M]^T [T^{***}] [M] - [B_v]^T p_w [B_v] + [M]^T [P] [M] + [B_v]^T \gamma_w [N]) dV$$

$$[K'] = \rho \int_{\Gamma_u} [N]^T [N] dS, \quad [K_v] = \int_V [N_h]^T [N_h] dV,$$

$$\{\Delta F\} = \Delta t \int_{\Gamma_\sigma} [N]^T \{\bar{s}_t\} dS, \quad \{\Delta \rho\} = \rho \int_{\Gamma_u} [N]^T \{\bar{v}\} dS,$$



(a) Geometry and boundary conditions (b) Initial collocation of the nodal points

Fig. 6. Description of the problem for the saturated column test.

Table 2  
Material parameters.

Compression index	$\lambda$	0.11
Swelling index	$\kappa$	0.04
Critical state parameter	$M$	1.42
Poisson's ratio	$\nu$	0.333
Initial void ratio	$e_0$	0.83
Initial volume ratio	$v_0 = 1 + e_0$	1.83
Initial consolidation stress (kPa)	$p'_0$	294

$$[T^{**}] = \begin{bmatrix} T'_{11} & 0 & T'_{12}/2 \\ 0 & T'_{22} & T'_{12}/2 \\ T'_{12}/2 & T'_{12}/2 & (T'_{11} + T'_{22})/4 \end{bmatrix}, [T^{***}] = \begin{bmatrix} T'_{11} & 0 & T'_{12} & 0 \\ 0 & T'_{22} & 0 & T'_{12} \\ T'_{12} & 0 & T'_{11} & 0 \\ 0 & T'_{12} & 0 & T'_{22} \end{bmatrix},$$

$$[B] = \begin{bmatrix} \frac{\partial N^1}{\partial x} & 0 & \dots & \frac{\partial N^z}{\partial x} & 0 \\ 0 & \frac{\partial N^1}{\partial y} & \dots & 0 & \frac{\partial N^z}{\partial y} \\ \frac{\partial N^1}{\partial y} & \frac{\partial N^1}{\partial x} & \dots & \frac{\partial N^z}{\partial y} & \frac{\partial N^z}{\partial x} \end{bmatrix},$$

$$[C] = [C_1] - [C_2], [C_1] = \begin{bmatrix} a + b & a & 0 \\ & a + b & 0 \\ \text{sym.} & & b/2 \end{bmatrix},$$

$$[C_2] = \frac{1}{e} \begin{bmatrix} (cS_{11} - d)^2 & (cS_{11} - d)(cS_{22} - d) & cS_{12}(cS_{11} - d) \\ & (cS_{22} - d)^2 & cS_{12}(cS_{22} - d) \\ \text{sym.} & & (cS_{12})^2 \end{bmatrix},$$

$$a = \tilde{K} - \frac{2}{3}\tilde{G}, \quad b = 2\tilde{G}, \quad c = \frac{\tilde{G}}{\tau}, \quad d = \tilde{K}\tilde{\beta}, \quad e = \tilde{G} + \tilde{K}\tilde{\beta}^2 + h,$$

$$[B_v] = \begin{bmatrix} \frac{\partial N^1}{\partial x} & \frac{\partial N^1}{\partial y} & \dots & \frac{\partial N^z}{\partial x} & \frac{\partial N^z}{\partial y} \end{bmatrix},$$

$$[M] = \begin{bmatrix} \frac{\partial N^1}{\partial x} & 0 & \dots & \frac{\partial N^z}{\partial x} & 0 \\ 0 & \frac{\partial N^1}{\partial y} & \dots & 0 & \frac{\partial N^z}{\partial y} \\ \frac{\partial N^1}{\partial x} & 0 & \dots & \frac{\partial N^z}{\partial x} & 0 \\ 0 & \frac{\partial N^1}{\partial y} & \dots & 0 & \frac{\partial N^z}{\partial y} \end{bmatrix},$$

$$[P] = \begin{bmatrix} p_w & 0 & 0 & 0 \\ 0 & p_w & 0 & 0 \\ 0 & 0 & 0 & p_w \\ 0 & 0 & p_w & 0 \end{bmatrix}, \quad \{T'\} = \begin{Bmatrix} T'_{11} \\ T'_{22} \\ T'_{12} \end{Bmatrix},$$

$$\{v^*\} = \{\Delta u^*\}/\Delta t, \quad \{\bar{v}\} = \{\Delta \bar{u}\}/\Delta t, \quad [N] = [0 \quad N^1 \quad \dots \quad 0 \quad N^z]$$

where  $\Delta t$  is the time interval,  $\Delta \bar{u}$  is the boundary value of the displacement, and  $[C]$  is the constitutive stiffness matrix corresponding to Eq. (26). The weak form of the continuity for pore water is discretized by approximating the pore water pressure. The stiffness equation is described as

$$-[K_v]\{\Delta u^*\} - (1 - \theta)\Delta t([K_h] + [K'_h])\{h^*\}_{t+\Delta t} = \{\Delta Q\} + \theta\Delta t[K_h]\{h^*\}_t - \{\Delta \beta\} \quad (27)$$

where

$$[K_v] = \int_V [N_h]^T [B_v] dV, \quad [K_h] = \int_V [B_h]^T [k] [B_h] dV, \quad (28)$$

$$[K'_h] = \beta \int_{\Gamma_h} [N_h]^T [N_h] dS, \quad (29)$$

$$\{\Delta Q\} = \Delta t \int_{\Gamma_q} [N_h]^T \bar{q} dS, \quad \{\Delta \beta\} = \beta \Delta t \int_{\Gamma_h} [N_h]^T \bar{h}_w dS, \quad (30)$$

$$[k] = \begin{bmatrix} k/\gamma_w & 0 \\ 0 & k/\gamma_w \end{bmatrix}, \quad [B_h] = \begin{bmatrix} \frac{\partial N^1_h}{\partial x} & \dots & \frac{\partial N^z_h}{\partial x} \\ \frac{\partial N^1_h}{\partial y} & \dots & \frac{\partial N^z_h}{\partial y} \end{bmatrix} \quad (31)$$

where  $\theta$  is the parameter of difference.

### 2.5. The stabilization term

As previously mentioned, mixed displacement-pressure formulations (e.g., finite element methods) produce locking phenomena

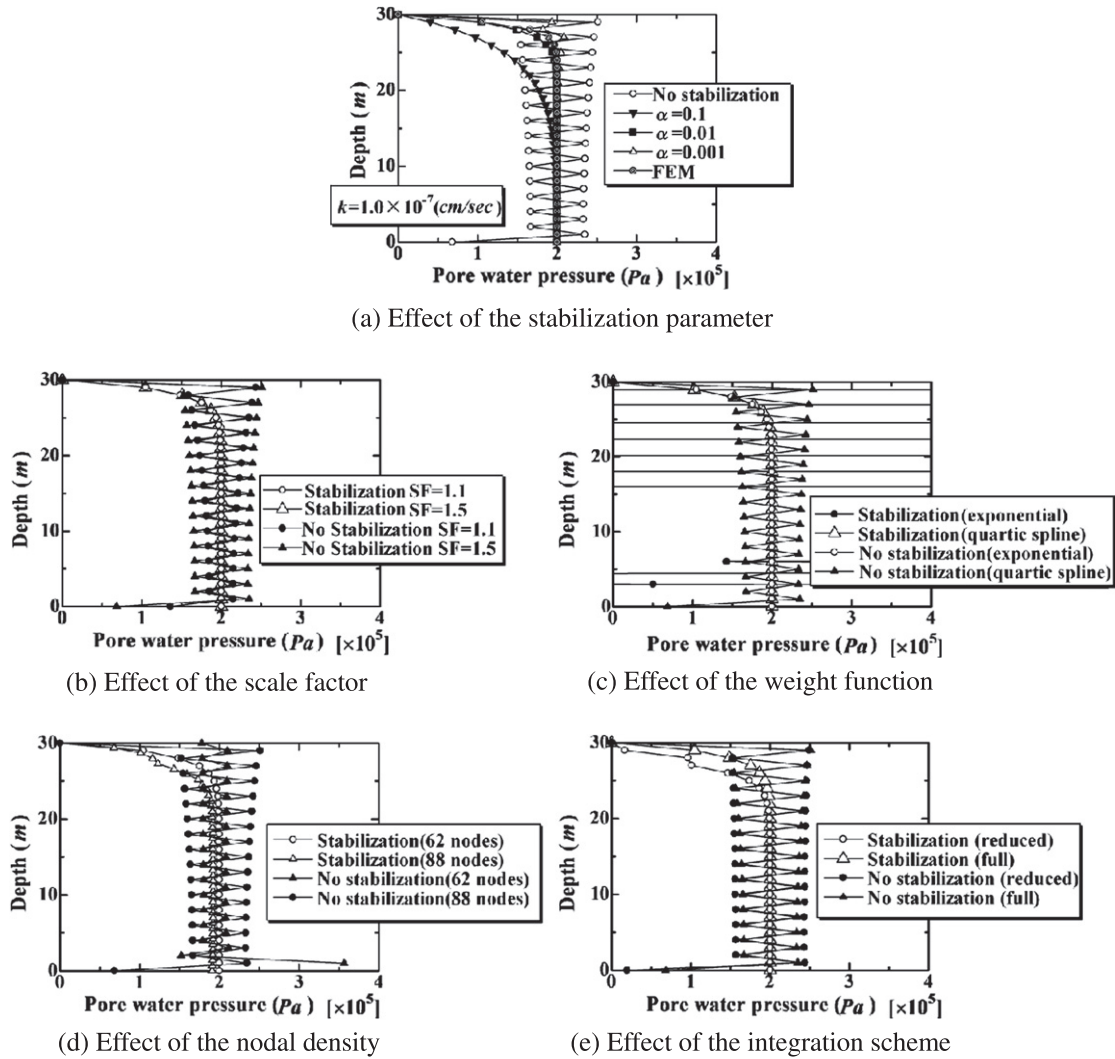
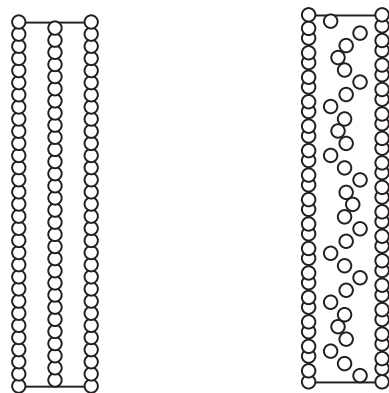


Fig. 7. Numerical results.



(a) Regular distribution (b) Irregular distribution

Fig. 8. Initial collocation of the nodal points.

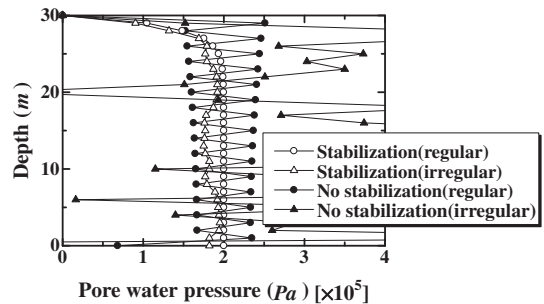


Fig. 9. Effect of the nodal distribution.

in the pressure field unless a stabilization technique is used. The remedy for such numerical instability has generally been to adopt a higher interpolation order for the displacements than for the pore pressure. As an alternative, however, an added stabilization term is incorporated.

It is shown in this study that the instability can be eliminated by adding the stabilization term which consists of the square of the pore water pressure of the first derivatives. The stabilization term is obtained by the shock capturing term using the Galerkin Least-Squares method for the continuity condition.

$$\begin{aligned}
 & - \int_V (\text{tr} \mathbf{D}) \delta h dV + \int_V v_w \cdot \text{grad} \delta h dV - \int_{\Gamma_q} \bar{q} \delta h dS \\
 & - \int_{\Gamma_h} \beta (p_w - \bar{p}_w) \delta h dS + \delta \int_V \alpha (p'_w)^2 dV = 0
 \end{aligned} \tag{32}$$

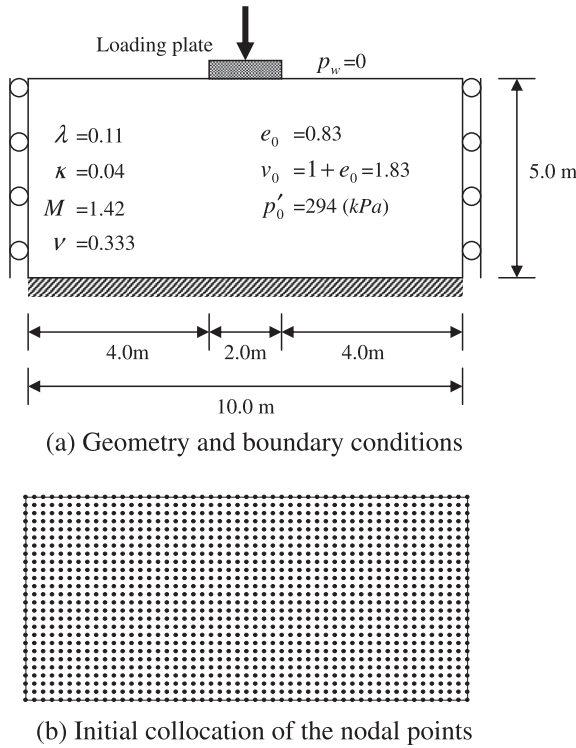


Fig. 10. Description of the problem.

where  $\alpha$  is the stabilization parameter,  $p'_w$  is the differentiate  $p_w$  with respect to  $x$  and  $z$ , and  $x$  is horizontal axis and  $z$  is vertical axis. We express the total head field as

$$h = [N_h^1 \dots N_h^\beta] \begin{Bmatrix} h^{*1} \\ \vdots \\ h^{*\beta} \end{Bmatrix} = [N_h] \{h^*\} \quad (33)$$

Differentiating matrix  $[N_h]$ , we obtain matrix  $[B']$  as

$$[B'] = \begin{bmatrix} \frac{\partial N_h^1}{\partial x} & \dots & \frac{\partial N_h^\beta}{\partial x} \\ \frac{\partial N_h^1}{\partial z} & \dots & \frac{\partial N_h^\beta}{\partial z} \end{bmatrix} \quad (34)$$

Substituting Eqs. (33) and (34) into the stabilization term, stabilization matrix  $[K_S]$  is shown as

$$[K_S] = \alpha \int_V [B']^T p_w [B'] dV \quad (35)$$

In this study, the soil column test created by Zienkiewicz et al. [27] is performed in order to examine the numerical stability of this procedure, and the values for the pore water pressure are illustrated along the vertical axis of the soil column. The two advantages of this stabilization procedure are as follows: (1) The interpolation order for the pore pressure is the same as that for the displacements, namely, a lower interpolation order is not adopted for the pore pressure. Therefore, the interpolation functions in the pore pressure field do not reduce the accuracy of the numerical results. (2) Table 1 summarizes the order of the interpolation functions for the pressure field and for the displacement field in FEM. The first derivatives of the interpolation functions in the pore pressure field are the zero order or the first order, as shown Table 1. Therefore, accuracy in the numerical results cannot be obtained. With EFG Method, however, the interpolation functions are derived by the MLS approximant and a linear-based polynomial is used, in other words, the resultant

interpolation functions are smooth. Moreover, when the distance between nodes tends to be zero,  $p'_w$  also tends to be zero.

Thus, the stabilization term,  $\delta \int_V \alpha (p'_w)^2 dV$ , also tends to be zero. The weak forms are integrated using the MLS interpolation function in space and the explicit time scheme in time. In order to obtain the integrals, background cells which are independent of the nodes are used, as shown in Fig. 2. In the manipulation of the stiffness matrix, a numerical integration is performed at the Gaussian points on the background cells. The interpolation function is calculated by the nodes in the domain. The background cells, which intersect or contact the boundary, are divided into four finer cells. The cells are then rearranged during the computation, according to changes in the domain, as shown in Fig. 3. In finite element method, the integration mesh is the same as the element mesh. In EFG, however, the background cell is required only in performing the integration of computing the stiffness matrix.

It is also necessary that, during the time evolution, the stress history is temporarily stored at the nodal points by transferring the stresses at the integration points through the interpolation function after evaluating the current stress state to construct the stiffness matrix, because the coordinates of the integration points are renewed along with the rearrangement of the background cells. Euler scheme is adopted for the stress update algorithms.

The curved boundary is dealt with in the similar manner for the normal boundary. Specifically, the background cells are divided into four finer cells, and the cells are rearranged during the computation, according to changes in the domain.

Herein, we describe the numerical implementation. First, the initial geometrical dimensions and the material properties of the domain with an allocation of the nodal points are defined. The initial displacements, the initial pore pressures at the nodal points, and the stress levels at the Gauss points, are set. Second, the background cells, the Gauss points and the boundary are determined. Here, the effective stress is resumed by the computation of the interpolation function and its derivative. The stiffness matrices are evaluated and assembled. After integration along the boundary, the stiffness equation is solved. Finally, the coordinates are renewed and the stresses at the nodal points are stored (see Fig. 4). Here, resultant stiffness equations are summarized in Fig. 5.

### 3. Numerical examples

#### 3.1. The saturated soil column test

For soil-water coupled problems, numerical instabilities are often encountered at the initial stage under undrained conditions unless a stabilization technique is performed. In this chapter, the numerical stability of an EFG computation is examined using the proposed stabilization term described in the last chapter. The body force is not considered in either the current or subsequent analyses.

Let's consider the 1D problem analyzed by Zienkiewicz et al. [27] in which the saturated soil column test in Fig. 6a uses the material parameters listed in Table 2. Here, a clay permeability of  $1.0 \times 10^{-7}$  cm/s is employed. A model discretized by 62 nodal points is adopted, as shown in Fig. 6b. Linear-based polynomials are applied for the interpolation functions of the EFG Method. The functions have the same order for both the displacements and the pore pressure. The weight function is a quartic spline type of weight function and its radius of support is 1.0. Here,  $5 \times 5$  Gaussian points are used. The background cells are 1.0 m within the domain and 0.5 m outside of the domain. The scale factor, which is defined as the magnification of the support diameter to the side length of the square background cell, is 1.5. This study employs penalty methods to apply the boundary conditions, and the

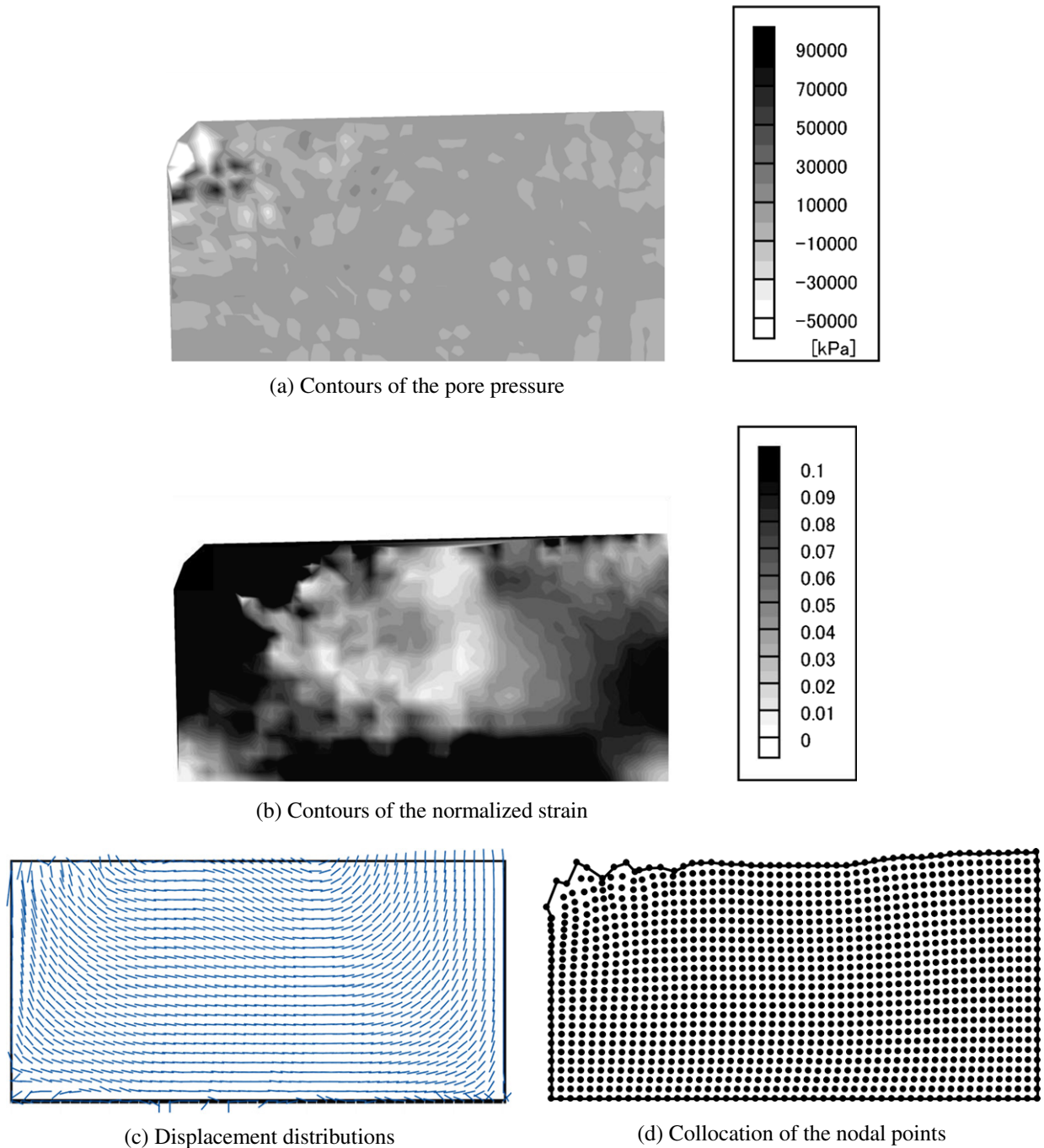


Fig. 11. Numerical results without stabilization term.

value of the penalty factor is  $1.0 \times 10^6$ . In order to solve the stiffness equation, the forward difference is adopted.

Fig. 7a shows the effect of the proposed stabilization term and dimensionless parameter  $\alpha$  in the numerical profile of the pore pressure just after loading under undrained conditions, for which a time difference of  $\Delta t = 0.01$  and a value of permeability of  $k = 1.0 \times 10^{-7}$  cm/s are adopted. There are 62 nodal points and the weight function is a quartic spline. The double circle line is the result analyzed by finite element method using the lower order interpolation function for the pore water pressure. From Fig. 7a, it can be concluded that the numerical solution has been improved in the case where the value of the dimensionless parameter is 0.01. In subsequent examinations, a permeability of  $1.0 \times 10^{-7}$  cm/s and a time difference of 0.01 are adopted.

The next examples we will consider are the effect of others conditions. Fig. 7b explains the effect of the scale factor. The values for the scale factor SF of 1.1 and 1.5 are adopted. Very good improvement of the results with the stabilization term is obtained. Fig. 7c shows the effect of the weight function. The quartic spline function and exponential function are employed as the weight function. From Fig. 7c, it can be seen from the figures that the numerical solution has been improved in any cases. The results for the effect of the nodal density can be seen in Fig. 7d. The total nodes of 62 and 88 are used. Again, good results for both nodes are observed. Results for the effect of the integration scheme are presented in Fig. 7e. The circle lines and the triangle lines show the results using reduced integration scheme and full integration scheme, respectively. It can be observed that the spurious pressure modes do

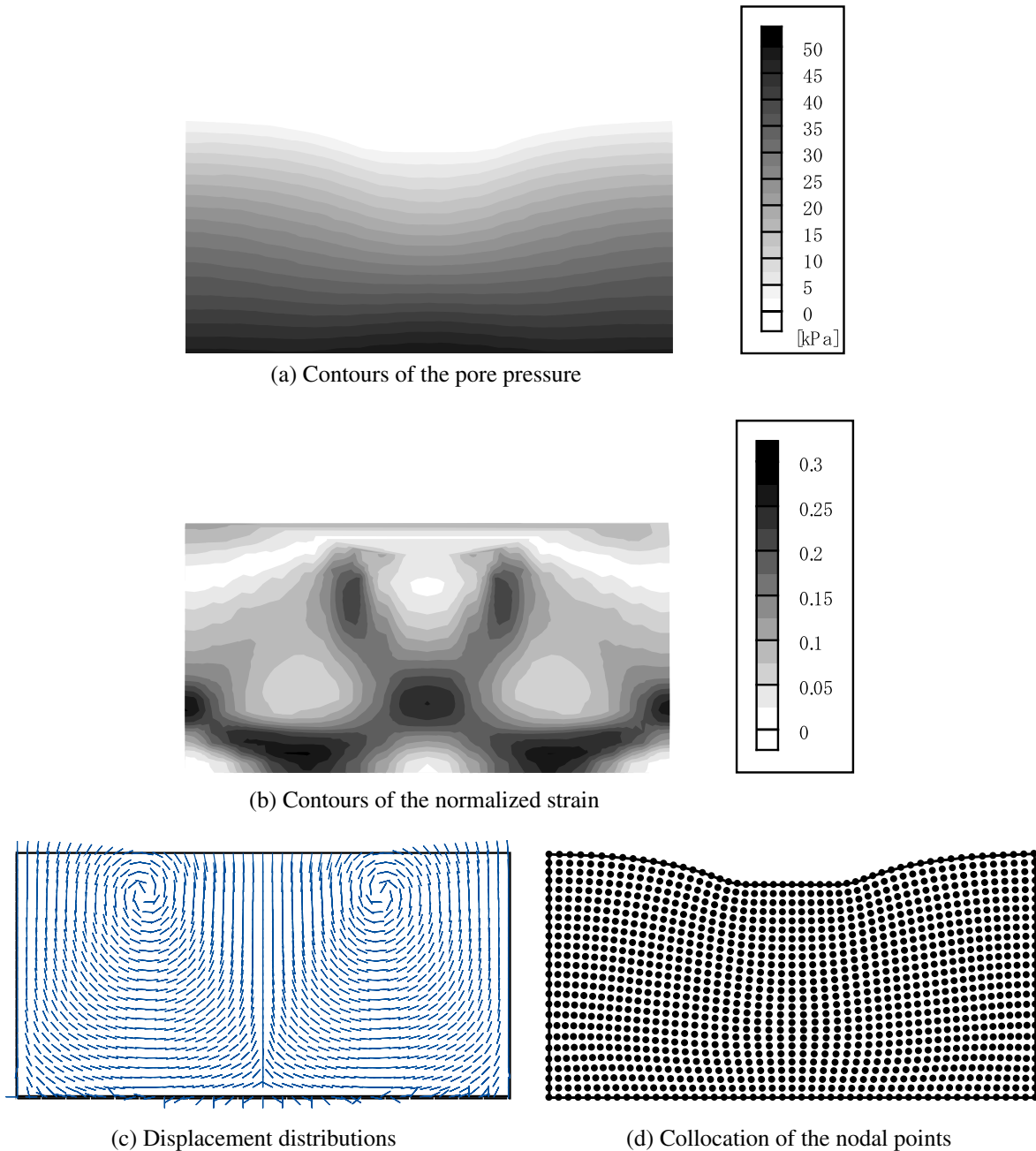


Fig. 12. Numerical results with stabilization term.

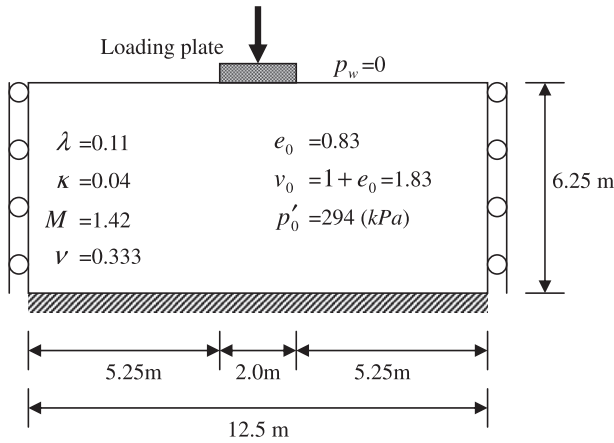
not occur if the stabilization term is considered. Next, two node distributions are shown in Fig. 8. The regular distribution and irregular distribution have 92 nodes. Fig. 9 shows the effect of irregularity on the nodal arrangement. The results of using the stabilization procedure are good in the cases.

Here, the numerical instability is caused by the large difference in the value of the stiffness matrix between the displacements and the pore water pressures. Generally, the values of the stiffness matrix for the pore water pressure are smaller than those for the displacements. However, if the lower order interpolation function in the pore water pressures is adopted, the values of the stiffness matrix for the pore water pressures become large, so that the difference in the values of the stiffness matrix becomes small. Similarly, if the stabilization term is considered, the values of the stiffness matrix in the pore water pressure also become large.

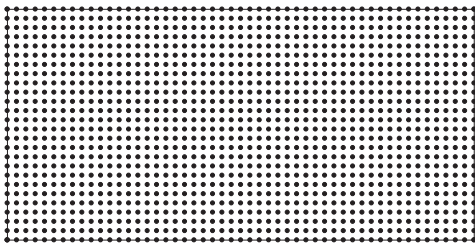
Therefore, the stabilization term using the forward difference quells the anomalous pore pressure behavior because of the small difference. However, EFG takes more calculation time compared with the finite element method because of the difference of the calculation procedure in the interpolation functions.

### 3.2. Foundation problem subjected to strip loading

In order to examine the numerical availability of the stabilization procedure to EFG Method, a 2D soil-water coupled problem is solved in relation to a soft soil foundation. The geometry and the boundary conditions are given in Fig. 10a, while the initial collocation of the nodal points is shown in Fig. 10b. Vertical displacements are applied at the top face to simulate loading on the foundation, while the transverse direction is restrained. Thus, the



(a) Geometry and boundary conditions



(b) Initial collocation of the nodal points

Fig. 13. Description of the problem #2.

boundary conditions under the loading surface are given by the settlements, and the other locations on the upper boundary are stress free. The bottom boundary is fixed in all directions, while the side boundaries are fixed in only the horizontal direction, such that vertical displacement is allowed. Hydrostatic pressure is used here for the initial conditions in the pore pressure field. The model is generated with 1326 nodal points, in other words, 26 vertical nodal points and 51 horizontal nodal points. The background cells are 0.2 m in size, and the value of dimensionless parameter  $\alpha$  is the same as in the previous analysis. Figs. 11 and 12 present the numerical results without and with the stabilization term, respectively, in which (a), (b), (c), and (d) show the contours of the pore water pressure, the contours of the normalized strain, the displacement distributions, and the collocation of the nodal points, respectively. In these results, the settlements under the loading surface are 0.04 m in Fig. 11 and 0.4 m in Fig. 12, respectively. The normalized strain measure is given as

$$\|\varepsilon\| = \sqrt{\text{tr}(\varepsilon\varepsilon^T)} \quad (36)$$

where  $\varepsilon = \int_0^t \mathbf{D}dt$  [28].

Spurious oscillations arise in the pore pressure field, as can be seen in Fig. 11a. In contrast to the results using the stabilization procedure, high values are obtained for the pore pressure and for the normalized strain in Fig. 11a and b, respectively. In particular, anomalous behavior appears on the left side in these figures. Moreover, the directions of the displacement vectors are disorderly in Fig. 11c because of the interaction between the pore pressure field and the displacement field. If a stabilization technique is used, however, no oscillations appear in the solution, as observed in Fig. 12. Fig. 12a accurately displays the rise in pore water pressure below the loading surface. In Fig. 12b, the prominently localized zones of the normalized strain occur just beneath the edge of the

loading surface. The deformed pattern in Fig. 12c is very similar to the classical slip line solution obtained by Prandtl. The shear bands are recognized as the localized deformation.

In order to consider the influence of the boundary for the failure surface, another model for the foundation problem is solved. The geometry and the boundary conditions are given in Fig. 13a and b. The width and the height of the model are 1.5 times the length of the original model and the material parameters are the same as those of the original model. Fig. 14a–d present the numerical results. The results concerning the failure surface are similar to the original results; therefore, the domain in the original computational model is suitable.

Fig. 15 compares the EFG solution with Prandtl's solution. Prandtl's solution  $q_f$  is expressed as

$$q_f = 5.14c_u \quad (37)$$

where  $c_u$  is the undrained shear strength.

Here, we briefly describe the undrained shear strength for the Cam-clay model [29]. The volume change of clay under undrained condition is expressed as follows

$$\varepsilon_v = \frac{\tilde{\lambda}}{1 + e_0} \ln \frac{p'}{p'_0} + D \frac{q}{p'} = 0 \quad (38)$$

The failure condition is written as

$$M - \frac{q}{p'} = \frac{\tilde{\lambda} - \tilde{\kappa}}{D(1 + e)} - \frac{q}{p'} = 0 \quad (39)$$

Substituting Eq. (38) into (39) gives

$$\frac{q}{p'} = M \frac{q}{p'_0} = M \exp\left(-\frac{\tilde{\lambda} - \tilde{\kappa}}{\tilde{\lambda}}\right) \quad (40)$$

Since the undrained shear strength is the half of the second invariant of deviatoric stress, we can obtain as

$$\frac{c_u}{p'_0} = \frac{M}{2} \exp\left(-\frac{\tilde{\lambda} - \tilde{\kappa}}{\tilde{\lambda}}\right) \quad (41)$$

From this figure, it is revealed that the EFG solution approaches Prandtl's solution, namely, the numerical result provides a reasonable solution profile. This result shows that the EFG method with the stabilizing procedure is capable of solving problems of computational geomechanics.

#### 4. Conclusion

In this paper, we have proposed a stabilization method for soil-water coupled problems using the Element-free Galerkin Method. A stabilization term has been presented by the addition of a continuity condition. The proposed stabilization procedure has the following two characteristics: (1) The interpolation order for the pore pressure field is the same as that for the displacements, in other words, a lower interpolation order for the pore pressure is not adopted. (2) The stabilization term consists of first derivatives in which the interpolation functions are smooth because of the MLS approximation. The saturated column test and the foundation loading problem have been solved using the stabilization procedure. Numerical examples have shown that the stabilization method can indeed quell the anomalous pore pressure behavior.

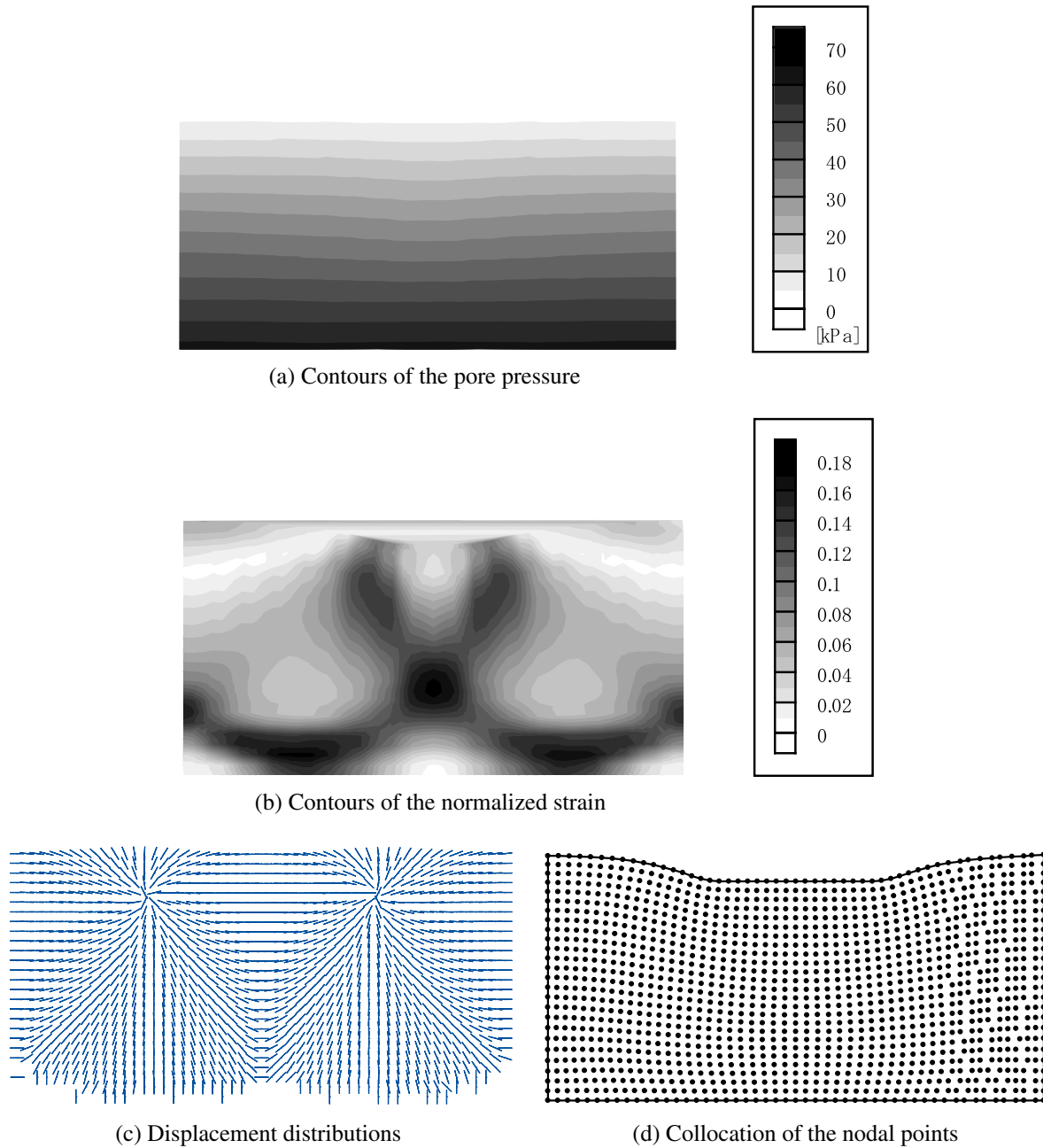


Fig. 14. Numerical results with stabilization term #2.

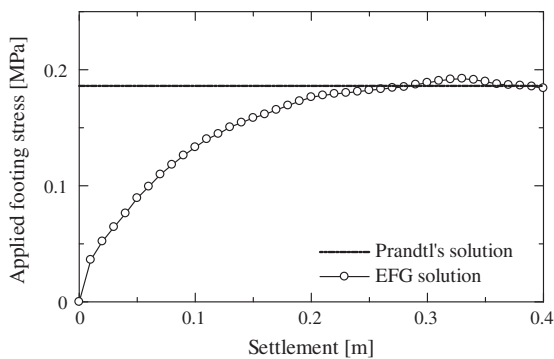


Fig. 15. Comparison EFG solution with Prandtl's solution.

**Acknowledgements**

This research was greatly inspired by Ted Belytschko. Professor Belytschko was kind enough to offer many useful suggestions. We would like to express our deep thanks to him.

**References**

- [1] Modaressi H, Aubert P. Element-free Galerkin method for deforming multiphase porous media. *Int J Numer Methods Eng* 1998;42:313–40.
- [2] Nogami T, Wang W, Wang JG. Numerical method for consolidation analysis of lumpy clay fillings with meshless method. *Soils Found* 2004;44(1):125–42.
- [3] Murakami A, Setsuyasu T, Arimoto S. Mesh-free method for soil-water coupled problem within finite strain and its numerical validity. *Soils Found* 2005;45(2).
- [4] Wang ZL, Li YC. Analysis of factors influencing the solution of the consolidation problem by using an element-free Galerkin method. *Comput Geosci* 2006;32:624–31.

- [5] Wang JG, Liu GR, Wu YG. A point interpolation method for simulating dissipation process of consolidation. *Comput Methods Appl Mech Eng* 2001;190:5907–22.
- [6] Wang JG, Liu GR, Lin P. Numerical analysis of Biot's consolidation process by radial point interpolation method. *Int J Solids Struct* 2002;39(6):1557–73.
- [7] Wang JG, Yan L, Liu GR. A local radial point interpolation method for dissipation process of excess pore water pressure. *Int J Numer Methods Heat Fluid Flow* 2005;15(6):567–87.
- [8] Chen JS, Wu CT, Chi L, Huck F. A meshfree method for geotechnical materials. *J Eng Mech* 2001;127:440–9.
- [9] Zhang JF, Zhang WP, Zheng Y. A meshfree method and its applications to elasto-plastic problems. *J Zhejiang University Science* 2005;6A(2):148–54.
- [10] Cai YC, Zhu HH, Xia CC. Meshless natural neighbor method and its application to complex geotechnical engineering. *Yanshilixue Yu Gongcheng Xuebao/Chinese J Rock Mech Eng* 2005;24(11):1888–94.
- [11] Karim MR, Nogami T, Wang JG. Analysis of transient response of saturated porous elastic soil under cyclic loading using element-free Galerkin method. *Int J Solids Struct* 2002;39:6011–33.
- [12] Sato T, Matsumaru T. Numerical simulation of liquefaction and flow process using mesh free method. *J Geotech Eng* 2006;813:89–101. in Japanese.
- [13] Wang JG, Karim MR, Lin PZ. Analysis of seabed instability using element free Galerkin method. *Ocean Eng* 2007;34(2):247–60.
- [14] Wang JG, Nogami T, Dasari GR, Lin PZ. A weak coupling algorithm for seabed-wave interaction analysis. *Comput Methods Appl Mech Eng* 2004;193:3935–56.
- [15] Wang JG, Zhang B, Nogami T. Wave-induced seabed response analysis by radial point interpolation meshless method. *Ocean Eng* 2004;31:21–42.
- [16] Rabczuk T, Areias PMA. A new approach for modeling slip lines in geological materials with cohesive models. *Int J Numer Anal Methods Geomech* 2006;30:1159–72.
- [17] Sheu GY. Direct back analysis by the meshless local Petrov-Galerkin method and Bayesian statistics. *Int J Numer Anal Methods Geomech* 2006;30(8): 823–42.
- [18] Chapelle D, Bathe KJ. The inf-sup test. *Comput Struct* 1993;47:537–45.
- [19] Pastor M, Li T, Liu X, Zienkiewicz OC. Stabilized low-order finite elements for failure and localization problems in undrained soils and foundations. *Comput Methods Appl Mech Eng* 1999;174:219–34.
- [20] Mira P, Pastor M, Li T, Liu X. A new stabilized enhanced strain element with equal order of interpolation for soil consolidation problems. *Comput Methods Appl Mech Eng* 2003;192:4257–77.
- [21] Wang WD, Wang JG, Wang AL, Nogami T. An unequal-order radial interpolation meshless method for Biot's consolidation theory. *Comput Geotech* 2007;34:61–70.
- [22] Khoshghalb A, Khalili N. A stable meshfree method for fully coupled flow-deformation analysis of saturated porous media. *Comput Geotech* 2010;37:789–95.
- [23] Hua L. Stable element-free Galerkin solution procedures for the coupled soil-pore fluid problem. *Int J Numer Methods Eng* 2010. doi:10.1002/nme.3087.
- [24] Asaoka A, Nakano M, Noda T. Superloading yield surface concept for highly structured soil behavior. *Soils Found* 2000;40(2):99–110.
- [25] Henkel DJ. The shear strength of saturated remoulded clay. In: Proceedings of research conference on shear strength of cohesive soils at boulder; 1960. p. 533–40.
- [26] Ohta H. Analysis of deformation of soils based on the theory of plasticity and its application to settlement of embankments. Doctoral Thesis, Kyoto University; 1971.
- [27] Zienkiewicz OC, Qu S, Taylor RL, Nakazawa S. The patch test for mixed formulations. *Int J Numer Methods Eng* 1986;23:1873–83.
- [28] Yatomi C, Yamashita A, Iizuka A, Sano I. Shear bands formation numerically simulated by a non-coaxial Cam-Clay model. *Soils Found* 1989;29:1–13.
- [29] Ohta H, Nishihara A, Morita Y. Undrained stability of  $K_0$ -consolidated clays. In: Proceedings 11th international conference on soil mechanics and foundation engineering, vol. 2; 1985. p. 613–6.